

# Large eddy simulation of gas-liquid flow in a bubble column reactor



"Stereo PIV arrangement in the bubble column considered in this work."

S. LAÍN\*

## Abstract

The dynamics of the gas-liquid flow developing in a cylindrical laboratory bubble column reactor is addressed using Eulerian-Lagrangian simulations. The three-dimensional unsteady simulations combine the Large Eddy Simulation (LES) turbulence model for describing the liquid phase and a Lagrangian approach for the gas (discrete) phase. The bubble equation of motion considers all the relevant forces, i.e., buoyancy, pressure, drag, added mass and transverse lift. From the calculations, the transverse lift in combination with the drag is identified as the main mechanism allowing the bubbles to spread over the column cross-section. The liquid and gas velocity profiles obtained are compared with the experimental data and  $k - \epsilon$  results presented in Lain *et al.* (2001). As a result, the dynamic structure of the liquid flow induced by the rising bubbles is well

\* Fluid Mechanics Research Group, Energetics and Mechanics Department. Universidad Autónoma de Occidente. Colombia. slain@uao.edu.co

Fecha de recepción: agosto 27 de 2008

Fecha de aceptación: noviembre 15 de 2008

reproduced and also good quantitative results for all measured variables of both phases, gas and liquid, are obtained.

**Key words:** Bubbles, two-phase flow, large eddy simulation, particle image velocimetry

### Resumen

En este artículo se aborda la descripción de la dinámica del flujo gas-líquido en el interior de una columna de burbujas de laboratorio de geometría cilíndrica mediante el esquema Euler-Lagrange. Las simulaciones tridimensionales no estacionarias combinan el modelo de turbulencia de Simulación de Grandes Escalas (LES) para describir la fase líquida y una aproximación Lagrangiana para la fase discreta gaseosa. La ecuación de movimiento de las burbujas considera todas las fuerzas relevantes, es decir, flotabilidad, presión, resistencia, masa añadida y sustentación transversal. Analizando los cálculos, las fuerzas más importantes para describir la migración transversal de las burbujas son la resistencia y la sustentación transversal. Los perfiles de velocidad obtenidos para las fases líquida y gaseosa se han comparado con los resultados obtenidos en Laín *et al.* (2001) con el modelo  $k-\epsilon$ . Como resultado, el patrón de flujo dinámico del flujo del líquido inducido por las burbujas se reproduce satisfactoriamente. También existe buen acuerdo cuantitativo para todas las variables medidas de ambas fases, gas y líquido.

**Palabras clave:** Burbujas, flujo bifásico, simulación de grandes escalas, velocimetría de imagen de partículas

### Introduction

Bubble columns are frequently encountered in the chemical, petrochemical and industries. For the sound design of this kind of devices in process engineering it is necessary to understand their fundamental hydrodynamic behaviour, which is determined by bubble rise, bubble-bubble and bubble-liquid interactions, bubble size and bubble size distribution, and gas hold-up. Moreover, fluctuations of velocity are induced in the liquid by the movement of the bubbles due to the shear produced in the vicinity of the bubbles, in particular due to bubble oscillations. However, while the time-averaged flow within a bubble column shows a very regular and symmetric structure, the transient flow behaviour is generally highly irregular and asymmetric. As the bubbles react to local and instantaneous flow patterns, the dynamic interactions among the bubbles

and between bubbles and liquid affect the performance of the column.

From the engineering point of view two approaches are mainly used to simulate flow in Hubble columns and in multiphase flow in general (for a review the reader is referred for instance to Jakobsen *et al.*, 1997). Euler-Euler approaches or two-fluid models treat the liquid and gas as two interpenetrating media, where conservation equations are required for each phase together with interphase exchange terms; the main advantage is the relatively low computational demands. However, sophisticated closures are required to describe bubble-fluid interaction as well as interactions between bubbles. For polydisperse bubbles (which is usually the case) moreover several sets of conservation equations have to be solved, which will remarkably also increase computational demands. The Euler-Lagrange procedure, on the other hand, solves the Newton's second law of motion for each bubble provided that the forces acting on each element are known; it is computationally more expensive than Euler-Euler approach but it has the advantage that bubble-bubble interactions and polydispersity are taken into account in a natural manner. In both strategies, the liquid phase is treated as a continuum so the bubble induced velocity fluctuations in the liquid have to be modeled somehow. During the last years the  $k-\epsilon$  model has been applied by various authors (e.g., Sanyal *et al.* (1999), Laín *et al.* (2002), Bourtloutski and Sommerfeld (2002)) to describe the fluctuating structure of the liquid velocity field getting promisingly good qualitative and quantitative agreement with experimental data obtained by PDA, PIV-PTV or CARPT techniques. Nevertheless, because of the low Reynolds number implied in the liquid motion, a Large Eddy Simulation (LES) description of the underlying liquid motion is conceptually more attractive than RANS turbulence models, originally developed for turbulent, high Reynolds number flows. A thorough review of the modeling of bubble induced liquid flows can be found in Laín (2007).

In fact, the use of LES for vertically driven flows has been suggested since several years ago (e.g., Jakobsen *et al.* (1997)). However, only recently bubble column simulations employing LES formulations have appeared in the literature under the Euler-Euler framework (Deen *et al.*, 2001; Milelli *et al.*, 2001) and using the Euler-Lagrange approach (van den Hengel *et al.*, 2003; Laín and Sommerfeld, 2004). The main conclusions of these studies were: first, relatively coarse grids could be used without losing any fundamental characteristics of the flow; second, the effect of bubbles on the liquid effective viscosity, the so-called bubble induced

turbulence, could be safely neglected and, finally, the transversal dispersion of the bubbles was driven by the transverse lift force.

This paper focuses on the transient simulation of the three-dimensional flow developing in a laboratory cylindrical bubble column. The liquid flow is described by means of Large Eddy Simulation whilst for the bubble phase a Lagrangian tracking is employed, i.e., an Euler-Lagrange scheme is adopted. The main difference with the previously cited works is that the bubbles are present in all the liquid domain instead of being a bubble plume. The results of the simulations are compared with the PIV experimental measurements and  $k-\varepsilon$  calculations presented in Laín *et al.* (2001).

### Flow configuration

The considered experiments were carried out at the chair of Mechanical Process Engineering at the Martin-Luther University Halle, Germany. The experimental set-up consists of a cylindrical laboratory bubble column with a diameter of 140 mm and a height of 650 mm (i.e., water level in the bubble column). Aeration was performed by means of a porous membrane with a diameter of 100 mm and pore sizes of  $0.7 \mu\text{m}$  pretending to establish a homogeneous aeration over the cross-section of the aerator. The gas flow rate could be varied through the supply pressure.

For analysing the bubble swarm behaviour and simultaneously evaluating the flow structure and bubble-induced turbulence in a bubble column Particle Image Velocimetry (PIV) was applied. A two-phase PIV-system was developed to evaluate instantaneous flow fields of both rising bubbles and the continuous phase (Figure 1). The measurement of the liquid velocities in the bubble swarm was done by adding fluorescing seed particles. Images of bubbles and fluorescing tracer particles were acquired by two CCD cameras. The signals from tracers and bubbles were separated by optical

interference filters with a band width corresponding to the emitting wavelength of the fluorescing tracer particles and the wavelength of the applied Nd-YAG pulsed laser, respectively. To improve the phase separation of the system, the CCD cameras were placed in a non-perpendicular arrangement with respect to the light sheet. Full details about the experimental facility and measurement technique can be found in Bröder and Sommerfeld (2002).

### Modelling and numerical approach

The three-dimensional dynamic simulations of the flow evolving in a bubble column have been performed using the Euler/Lagrange approach by means of the combination of the finite volume code FASTEST and LAG3D solvers (Decker, 2005). The liquid flow is calculated by using the time-dependent filtered Navier-Stokes equations, i.e., Large Eddy Simulation (LES). Therefore, the three-dimensional equations of continuity and momentum extended by accounting for the effects of the dispersed (gas) phase are considered. They can be written in tensorial notation as (where the comma followed by a subscript means partial derivative and summation is performed over repeated indexes):

$$\hat{\rho}_{,i} + (\hat{\rho} \hat{u}_i)_{,i} = 0 \quad (1)$$

$$(\hat{\rho} \hat{u}_j)_{,i} + (\hat{\rho} \hat{u}_i \hat{u}_j)_{,i} = -\hat{p}_{,j} + \left( \mu_{\text{eff}} (\hat{u}_{i,j} + \hat{u}_{j,i}) - \frac{2}{3} \mu_{\text{eff}} \hat{u}_{k,k} \delta_{ij} \right) + \hat{\rho} g_j + F_{IB} \quad (2)$$

where the hat ( ^ ) indicates filtered variables. Here,  $\rho$  is the liquid density,  $u_j$  is the liquid velocity which is decomposed in a resolved part  $\hat{u}_j$  and the sub-grid scale (SGS) part  $u_j^{\text{SGS}}$ ,  $p$  is the liquid pressure and  $g_j$  is the respective component of the gravity acceleration. In Equation (2),  $\mu_{\text{eff}}$  is the effective viscosity for the liquid which is composed of two contributions: the molecular viscosity  $\mu_l$  and the so-called turbulent viscosity  $\mu_t$ :

$$\mu_{\text{eff}} = \mu_l + \mu_t \quad (3)$$

The turbulent viscosity simulates the contribution of the subgrid scales and in this work it is

described by the Smagorinsky model (Smagorinsky, 1963), which is essentially an eddy viscosity model. Therefore, this sub-grid scale viscosity is expressed as:

$$\mu_t = \hat{\rho} (C_s \Delta)^2 \sqrt{2 \hat{S}_{ij} \hat{S}_{ij}} \quad (4)$$

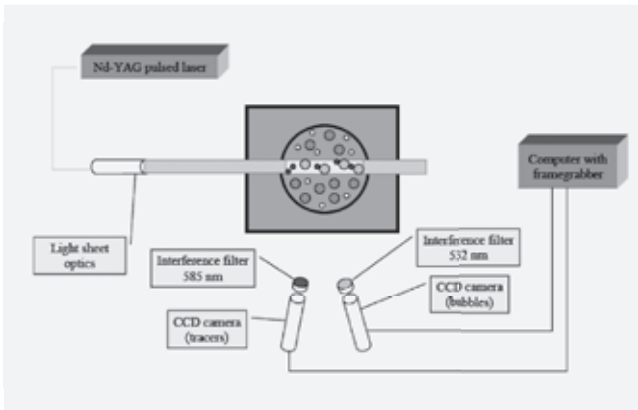


Figure 1. Two-phase PIV-system.

where  $\hat{S}_{ij}$  is the symmetric deviatoric part of strain tensor of the resolved scales. It is written as:

$$\hat{S}_{ij} = \frac{1}{2}(\hat{u}_{i,j} + \hat{u}_{j,i}) \quad (5)$$

In Eq. (4)  $C_s$  is the Smagorinsky constant whose value ranges in the literature from 0.065 up to 0.2, and  $\Delta$  is the filter width. The last term in Equation (2)  $F_{ib}$ , the momentum interaction term, represents the action of the bubble phase on the liquid phase by means of the interface forces which will be discussed below. Since at present only low void fractions are considered, lower than 2% in all the considered cases, the liquid density is assumed to be unaffected by the presence of the bubbles. Therefore, hereafter we write  $\rho \equiv \hat{\rho}$ .

Time integration of the Eulerian equations is performed by a second-order full implicit method in order to decrease the truncation error in time, whilst a central differencing scheme is used for spatial discretisation of the liquid evolution equations. The simulation of the bubble phase by the Lagrangian method requires the solution of the equation of motion for each computational bubble (representing a parcel of a number of real bubbles with identical properties). The bubble motion after injection is calculated by solving the following set of ordinary differential equations:

$$\begin{aligned} \frac{dx_{Bi}}{dt} &= u_{Bi} \quad (6) \\ m_B \frac{du_{Bi}}{dt} &= \frac{3}{4} \frac{\rho}{\rho_B D_B} m_B C_D (u_i - u_{Bi}) |\vec{u} - \vec{u}_B| \\ &+ m_B g_i \left(1 - \frac{\rho}{\rho_B}\right) \\ &+ C_{VM} m_B \frac{\rho}{\rho_B} \left(\frac{Du_i}{Dt} - \frac{du_{Bi}}{dt}\right) \quad (7) \\ &+ C_{TL} \frac{\rho}{\rho_B} \varepsilon_{ijk} \varepsilon_{klm} (u_j - u_{Bj}) \frac{\partial u_l}{\partial x_m} \\ &+ m_B \frac{\rho}{\rho_B} \frac{Du_i}{Dt} \end{aligned}$$

including, from left to right, the forces of inertia, drag, weigh-buoyancy, virtual mass, transverse lift and fluid stress. Other forces such as the Basset history term are assumed to be negligible.

Here,  $x_{Bi}$  are the coordinates of the bubble position,  $u_{Bi}$  are the velocity components,  $D_B$  is the bubble

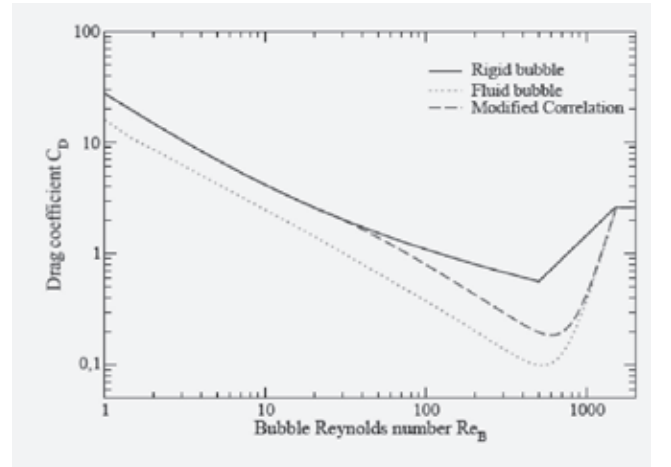


Figure 2. Drag correlation used in this work for rigid and fluid bubbles .

diameter, and  $\rho_B$  is the gas density which is assumed to be constant at present. The symbol  $\frac{D \bullet}{Dt}$  means the derivative following the fluid element.  $\varepsilon_{ijk}$  are the components of the Levi-Civita pseudo-tensor (equal to 1 when  $ijk$  is an even permutation of 123, -1 when the permutation is odd, and zero when any two indexes have the same value), which are used to express the curl or the cross product of vectors.

The drag coefficient  $C_D$  is calculated using a modified empirical correlation:

$$C_D = \begin{cases} 24 Re_B^{-1} (1 + 0.15 Re_B^{0.687}) & Re_B < 500 \\ 9.5 \times 10^{-5} Re_B^{1.397} & 500 \leq Re_B < 1500 \\ 2.61 & 1500 \leq Re_B \end{cases} \quad (8)$$

where  $Re_B = \rho D_B |\vec{u} - \vec{u}_B| / \mu_l$  is the bubble Reynolds number. As it can be seen from Figure 2 this correlation corresponds to the rigid bubble drag law for low Reynolds numbers and tends to the fluid bubble drag law for Reynolds numbers larger than 1000. The transverse lift coefficient  $C_{TL}$  appearing in the bubble equation of motion (7) is based on the correlation proposed by Tomiyama (1998):

$$C_{TL} = \begin{cases} \min\{0.288 \tanh(0.121 Re_B), f(Eo)\} & Eo < 4 \\ f(Eo) & 4 \leq Eo < 10 \\ -0.29 & Eo \geq 10 \end{cases} \quad (9)$$

where  $Eo$  is the Eotvos number defined as:

$$Eo = \frac{g(\rho - \rho_B) D_B^2}{\sigma}$$

$\sigma$  being the air/water surface tension coefficient and

$$f(Eo) = 0.00105Eo^3 - 0.0159Eo^2 - 0.0204Eo + 0.474$$

The above equation (9) gives  $0 < C_{TL} < 0.288$  for small bubbles that migrate towards the wall and negative values for large distorted bubbles. Following Tomiyama, for an air-water system under atmospheric pressure and room temperature,  $C_{TL}$  changes its sign for a bubble size of  $D_B = 5.6$  mm, which is well enough above the maximum bubble diameter considered in this work, i.e.  $D_B = 2.6$  mm. It is necessary to point out that the values of  $C_{TL}$  are below the factor 0.5 used in some other works (e.g., Deen *et al.* (2001), van den Hengel *et al.* (2003)). Also, Legendre and Magnaudet (1997), carrying out a theoretical analysis of forces acting on a spherical bubble in a low Reynolds number shear flow, found values of  $C_{TL}$  above those provided by eq. (9) which tends to 0.5 for larger bubble Reynolds numbers.

In our present air-water system  $Eo < 0.14$  for bubbles with diameter below 1 mm., which means that we are in the surface tension dominant regime and, therefore, the shape of those bubbles is approximately spherical. In consequence, for the smaller bubbles (i.e., below 1 mm.) we will take the transverse lift coefficient as 0.5, accordingly with the previous cited works, but for bubbles of larger diameter (presumably distorted) the Tomiyama correlation (9) will be used.

On the other hand  $C_{VM}$  is the virtual mass coefficient, which is taken equal to 0.5 through this paper.

The bubble equation of motion (7) is analytically integrated by assuming that the forces such as gravity and buoyancy, virtual mass, transverse lift and pressure term are constant during the time step. The numerical solution requires that the time step of integration (i.e. the Lagrangian time step  $\Delta t_L$ ) is sufficiently smaller than all relevant time scales for the bubble motion. In the considered vertical bubble-driven flow, the limiting time scale is mostly the bubble response time scale:

$$\tau_B(C_D) = \frac{4}{3\mu_l} \frac{(\rho_B + 0.5\rho)D_B^2}{Re_B C_D (Re_B)} \quad (10)$$

In order to avoid numerical instabilities, the time step was limited to be 25 % of the minimum of the above time scale (Lain and Göz, 2001). For improving numerical efficiency the Lagrangian time step was not fixed, but allowed to vary along the bubble trajectory.

### Effect of bubbles on liquid flow

Since the liquid flow in the bubble column is driven by the bubble rise, the source terms due to the bubble phase are essential. As both phases are computed time-

dependent, the evaluation of the source terms and the coupling between the phases requires some special treatment in order to yield reasonable averages of the source terms for each control volume, in which bubbles are present.

The selected Eulerian time step ( $\Delta t_E$ ) determines the temporal resolution of the flow fluctuations and its upper limit is given by the constraint that the maximum Courant-Friedrichs-Levy (CFL) number must be less than one. Moreover, in order to get appropriate temporal averaging of the source terms the Lagrangian time step ( $\Delta t_L$ ) for calculating the bubble trajectories should be generally much smaller.

The calculation of the interaction terms is realized by means of the Particle-source-in-cell (PSI-cell) approximation of Crowe *et al.* (1977). In the LES scheme adopted here, this model considers the dispersed phase as a local source of momentum. In this context, the expression for the momentum equation source term due to the bubbles is obtained by time- and ensemble averaging in the following form (Gouesbet and Berlemont, 1999):

$$F_{iB} = -\frac{1}{V_{cv}\Delta t_E} \sum_k m_k N_k \sum_n \left\{ \left( [u_{Bi}]_k^{n+1} - [u_{Bi}]_k^n \right) - g_i \left( 1 - \frac{\rho}{\rho_B} \right) \Delta t_L \right\} \quad (11)$$

where the sum over  $n$  indicates averaging of the instantaneous momentum contributions along the bubble trajectory (i.e. time averaging) and the sum over  $k$  is related to the number of computational bubbles passing through the considered cell of size  $V_{cv}$ . The mass of an individual bubble is given by  $m_k$ , while  $N_k$  is the number of real bubbles contained in one computational bubble. In (11) only the interfacial forces have to be taken into account, so the external forces have to be subtracted.

Following the PSI-Cell strategy, the coupling terms are introduced only within the cell where the centre of gravity of the bubbles is located. Let us remark that in Eq. (11) the temporal change of the instantaneous particle velocity is taken instead of the forces acting on such particle, because from a Lagrangian perspective this is easier and automatically all forces are accounted for.

### Numerical simulations

At this point it is very useful to summarize some results and conclusions obtained by other authors in similar configurations of bubbly flows employing the LES strategy for the liquid phase.

Regarding the grid size, Deen *et al.* (2001) and van den Hengel *et al.* (2003) conclude that, for vertical

bubble-driving flows, relative coarse grids can be used without losing any fundamental characteristics of the flow. For instance, Deen *et al.* (2001) report calculations in a square crosssectioned bubble column of  $0.15 \times 0.15 \times 1 \text{ m}^3$  using meshes of  $15 \times 15 \times 100$  and  $32 \times 32 \times 100$  cells without any significative differences between them. The study of Milelli *et al.* (2001) on a bubble plume developing in a cylindrical bubble column presents similar conclusions. In addition Milelli *et al.* (2001) show that for the case of a shear layer laden with bubbles it was also possible to provide an optimum filter width  $1.2 < \Delta / D_b < 1.6$ . However, this result was not fully supported for the bubble plume, where a coarser grid improved the results in the vertical direction. The constraint imposed on the ratio  $\Delta / D_b$  implied that the interaction of bubbles with the smallest resolved scales is captured without additional approximation. In practice, this condition conflicts with the fact that the computational grid should be large enough when compared to the bubble diameter in order to provide significant statistical samples (Tran, 1997).

The approach adopted here is to establish a grid size larger than bubble diameter but such that the ratio  $\Delta / D_b$  is not very far away from 1.6. Consequently, two grids have been considered in this work: a coarse one with  $29 \times 29 \times 50$  cells and a refined one with  $29 \times 29 \times 150$  cells which gives for the maximum bubble diameter of 2.6 mm a ratio  $\Delta / D_b \cong 1.8$  (bubble column diameter 140 mm and height 650 mm).

Regarding the bubble tracking, in the general case, the instantaneous fluid velocity at the bubble location occurring in Eq. (7) is determined from the local resolved fluid velocity  $\hat{u}_j$  linearly interpolated from the neighbouring grid points and a sub-grid root mean square velocity contribution  $u_j^{SGS}$ . Van den Hengel *et al.* (2003) found that for the case of a monodispersed bubble plume developing in the previously mentioned square cross-sectioned bubble column the effect of considering  $u_j^{SGS}$  in the bubble motion equation was negligible in the liquid variables.

This fact was due to the low effective Reynolds number of the liquid flow developing in this kind of bubble-driven flow systems. Therefore, nearly all the liquid energy is contained in the resolved scales which are provided by LES. Unfortunately, no information is given in that paper about the influence of the liquid subgrid rms velocity on the bubble velocities. Similar behaviour was encountered by Deen *et al.* (2001) and Milelli *et al.* (2001) using an Euler-Euler or two-fluid approach. The same approach was taken in the previous work of Laín and Sommerfeld (2004).

However, in this paper also the following simple model for the consideration of the subgrid scale fluctuating liquid velocity effects has been tested:

$$u_j^{SGS} = \xi_j \sqrt{\frac{2}{3} k^{SGS}} \quad (12)$$

where  $\xi_j$  is an independent random number sampled from a Gaussian distribution with zero mean and unit variance. On the other hand, the turbulent kinetic subgrid scale  $k^{SGS}$  is taken following the estimation of Lilly (1967):

$$k^{SGS} = \frac{(u_t / \rho)^2}{(0.094 \Delta)^2} \quad (13)$$

A further conclusion of the previously mentioned research is that the values adopted for  $C_{\tau}$  influence significantly the performance of the LES simulation. If the transverse lift was neglected, the bubbles did not experience any transversal spreading. This fact could be expected because in absence of transport by velocity fluctuations (or being that not significant), the only way of achieving bubble dispersion is due to the transverse lift force. Nevertheless, the values for  $C_{\tau}$  are different: 0.5 in Deen *et al.* (2001) and van den Hengel *et al.* (2003), and 0.25 in Milelli *et al.* (2001). The dependence of the bubble dispersion with the value of  $C_{\tau}$  has been also observed in Laín and Sommerfeld (2004) where the correlation proposed by Tomiyama (9) was adopted. However, in that work a bubble velocity peak near of the wall was obtained. This fact was explained by those authors who argue that the larger bubbles, having a higher slip velocity than the smaller ones, tended to migrate faster towards the wall resulting finally in a bubble velocity profile which had a maximum near the wall region. In addition, the liquid fluctuating velocity showed very low values when compared to experiments.

As it has been previously stated, the cylindrical bubble column of diameter 140 mm and height 650 mm was discretised by employing two grids: a coarse one with  $29 \times 29 \times 50$  cells and a refined one with  $29 \times 29 \times 150$  cells, the latter to check the influence of grid size in the results. The boundary conditions employed for the liquid phase were:

- no-slip boundary conditions at the walls
- the free surface of the bubble column was also specified as a wall boundary condition, which implies a no-slip condition.

The bubbles were injected just above the bottom of the bubble column over a cross-section with a diameter

of 100 mm according to the experiments. The gas phase mass flux was constant across the aerator. The size of the bubbles was sampled stochastically from the measured size distribution. The initial bubble velocity was sampled from a Gaussian distribution with a mean and rms-value corresponding to the measurements. At the free surface the bubbles are leaving the computational domain. The bubble-wall interactions are modelled as a perfectly elastic collisions.

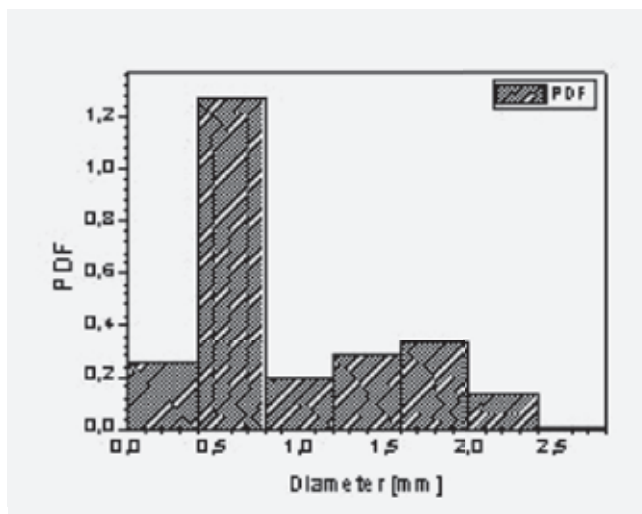


Figure 3. Computational bubble size distribution considered.

The calculation procedure is briefly summarised in the following. Firstly, the bubbles are randomly injected at the inlet area and tracked in quiescent liquid for a duration corresponding to the Eulerian time step in order to evaluate the source terms described above. During this first step of the start-up period of course the bubbles do not yet reach the surface of the column. The source terms are used to calculate the fluid flow field until a converged solution is achieved. Then the Lagrangian tracking with injecting new bubbles in each Eulerian time step is continued. With the new source terms the flow field at the next time level is calculated and so forth. It should be mentioned that with this unsteady procedure no under-relaxation of the source terms should be used.

The experimental case considered is the case 1 presented in Laín *et al.* (2001). The superficial gas velocity was 0.272 cm/s, the volume flow 151 l/h, the air voidage 1.46 % and the range of measured bubble diameters was [0.2, 2.6] mm with a mean bubble diameter of 0.92 mm. (Figure 3).

This case has been chosen because the extension of the  $k - \varepsilon$  model presented in Laín *et al.* (2002) was not able to provide simultaneously good agreement for the liquid mean vertical velocity and turbulent kinetic energy (Laín *et al.*, 2001) despite the fact that the model

performed good enough for operating conditions with smaller bubble sizes. The main idea of using LES for this kind of bubbly flows results from the expectation that the large scale motions (which carry most of the energy) would be primarily responsible for the macroscopic influence of the liquid velocity fluctuations on the bubble motion, including dispersion, whereas small-scale fluctuations would be less important, affecting more the localized bubble oscillations. Therefore, there is a hope that the statistics of velocity fluctuations induced in the liquid by the bubbles motion could be reasonably reproduced. In the following, the performance of LES in the considered configuration, in connection with a Lagrangian scheme for the gas phase, is evaluated.

The choice of the Eulerian time step,  $\Delta t_E$ , is determined by the criterium that the maximum Courant-Friedrichs-Levy (CFL) number must be less than one. Because of the low velocities induced in the liquid by the rising bubbles it has been checked that a value of  $\Delta t_E = 0.05$  s is enough to satisfy the requirement  $CFL < 1$ . However, during this investigation it was observed that the magnitude of the liquid fluctuating velocity depends on the value of  $\Delta t_E$ . Therefore, reducing the Eulerian time step results in an increase of the fluctuating liquid velocity. Fortunately, the changes of this variable when  $\Delta t_E$  was reduced below 5 ms. were very small, which was explicitly checked using  $\Delta t_E = 2.5$  ms.

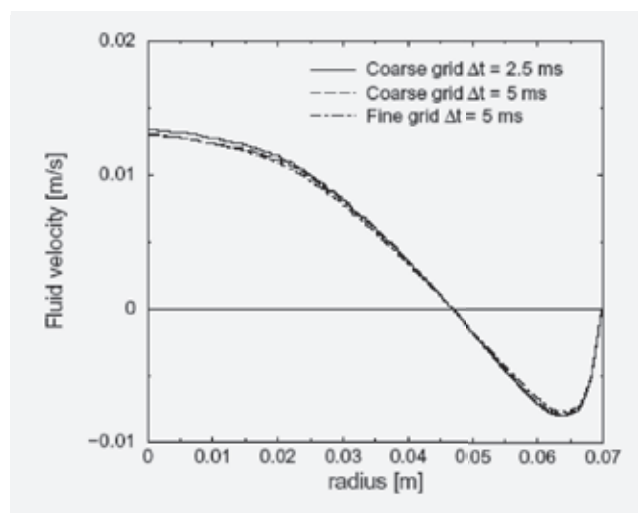


Figure 4. Influence of the Eulerian time step  $\Delta t_E$  and grid size on the time averaged vertical fluid velocity ( $z = 450$  mm.)

The evolution of the quasi-steady flow in the bubble column begins when the first bubbles leave the column. Normally this situation is reached after about 10 s. After that the data are time averaged up to the end of the simulation. At this stage typically 60.000 computational bubbles are included in the entire liquid domain. The flow is simulated usually during 250 s, but some

simulations have been run up to 500 s to be sure that the statistical steady state had been reached. In this case, 336 hours of CPU time were necessary in a PC Pentium 4 at 1.8 GHz with one processor.

The effect of the Eulerian time step  $\Delta t_e$  and grid size on the averaged vertical fluid velocity is investigated in Figure 4. The velocity profile corresponds to the section 450 mm above the aerator and it has been both, time and azimuthally, averaged. Time average (denoted by an overbar) is performed in each time step as:

$$\overline{u_i^n} = \frac{n - n_0 - 1}{n - n_0} \overline{u_i^{n-1}} + \frac{1}{n - n_0} u_i^n \quad (14)$$

where the average is started at time step  $n_0$ . After that, the velocities at each vertical crosssection are averaged in the angular coordinate, providing a velocity profile versus the radial coordinate.

When the Eulerian time step is fixed  $\Delta t_e = 5$  ms, Figure 5 shows that the results for the fluid velocity are almost independent of the grid size. On the other hand, the changes in the velocity profile when the Eulerian time step is halved, using the coarse grid, are quite small. In all the cases the requirement of  $CFL < 1$  is satisfied. Therefore, the following simulations have been performed in the coarse grid with an Eulerian time step of  $\Delta t_e = 5$  ms. In all these cases the value for the Smagorinsky constant  $C_s = 0.1$  and the modified drag law for bubbles (8) have been adopted.

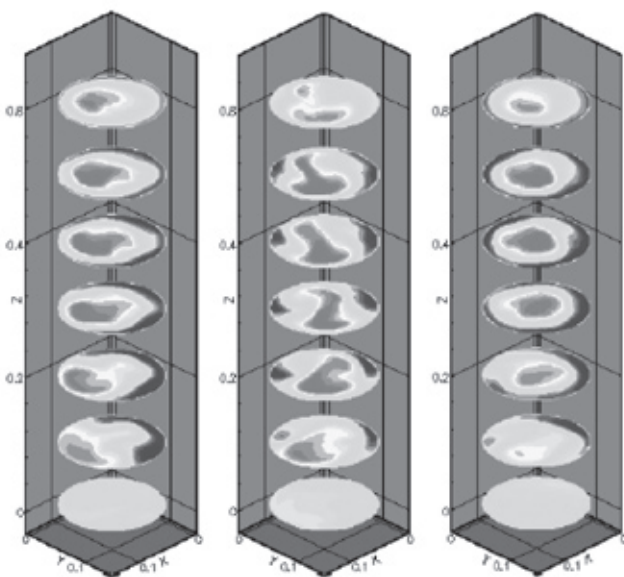


**Figure 5.** Instantaneous liquid vertical velocity contours for three different times: 125 s (left), 150 s (center) and 175 s (right).

## Results

The typical temporal evolution of the flow structure in the bubble column is shown in Fig. 5 by plotting contours of the (resolved) instantaneous vertical velocity at three different equidistant times. The red color in the slices indicates upwards velocities and blue color downwards velocities. In general, the over-all flow pattern consists of a large recirculating loop where the flow is directed upwards in the center of the column and downwards near of the walls. It can be seen that some areas, which change with time where the liquid rises near the wall, especially in the region immediately above the aerator. Eventually, the average over a long enough time period gives the usual recirculation pattern (liquid rises in the center and goes down near the walls).

In the following, the time and azimuthally averaged velocity profiles versus radius, for both phases at several cross-sections  $z = 33, 110, 308, 495$  mm above the aerator, are considered.

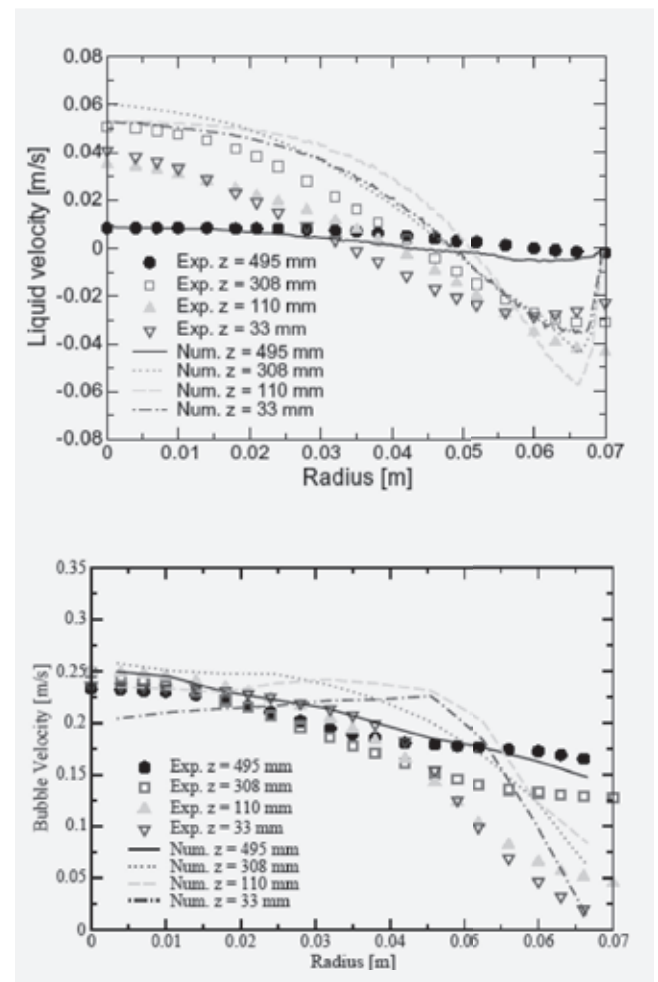


**Figure 6.** Mean vertical fluid velocities (top) and vertical bubble velocities (bottom) in four cross-sections of the bubble column  $z = 33, 110, 308, 495$  mm.



Figures 6 and 8 shows the results of simulations using the modified bubble drag law (8) and the transverse lift coefficient,  $C_{TL}$ , which has been taken as 0.5 for small bubbles, with diameter below 1 mm., and according to the Tomiyama (1998) correlation (9) for the larger bubbles. As it has been previously mentioned the correlation for  $C_{TL}$  is motivated for the low  $EO$  values for the air-water system, which support the hypothesis of the spherical shape for the smaller bubbles, and the theoretical results of Legendre and Magnaudet (1997). Figure 6 shows the mean velocity profiles for liquid (top) and bubbles (bottom) in four cross-sections of the bubble column at  $z = 33, 110, 308, 495$  mm above the aerator. The liquid velocities induced by the bubble rising in this case presents a nearly flat profile near of the centre-line and then velocities decrease gradually to negative values in the zone of downflow and reach eventually the zero value on the wall. As it can be readily seen in that figure, the agreement of the liquid velocity with the measurements improves as we ascend in the bubble column, being the comparison at  $z = 495$  mm quite good. There are some quantitative discrepancies in the lower cross-sections but the tendence shown by the calculations agrees very well with that shown in the experiments, i.e., the center line mean liquid velocity is very similar in the two first sections,  $z = 33, 110$  mm, increases in the third section and decreases again in the upper one of  $z = 495$  mm.

On the other hand, the bubbles mean velocity agrees reasonably well with the measurements at the four cross-sections, being quite good for the upper section at  $z = 495$  mm. above the aerator. It is important to stress that no gas velocity peak is observed near the wall, mainly due to the fact that the mean bubble diameter is roughly constant over the entire cross-section. The combination of the proposed modified bubble drag (8) and the transverse lift coefficient, previously mentioned, allows to keep an even distribution of bubble diameters over each cross-section accordingly with the experiments (Figure 7).

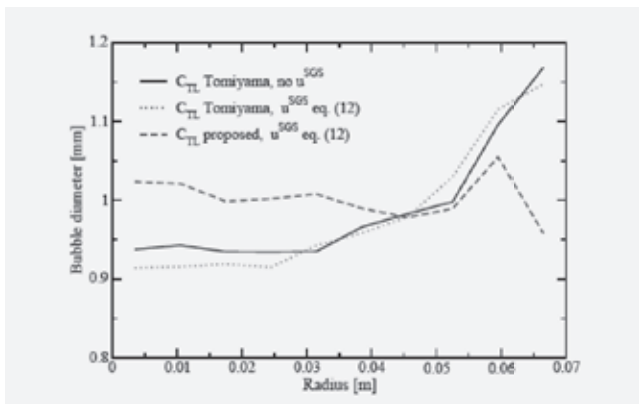


**Figure 7.** Influence of the transverse lift coefficient formulation and effect of the subgrid root mean square velocity  $u^{SGS}$  on the distribution of bubble diameter over the crosssection  $z = 495$  mm. above the aerator.

This behaviour was not achieved using only the Tomiyama (1998) correlation because the transverse lift coefficient for the smallest bubbles (with the smallest bubble Reynolds numbers) tends to zero as the bubble diameter decreases. Figure 7 shows how the Tomiyama correlation produces a larger bubble mean diameter near of the wall compared to the proposed correlation, which gives a more even distribution. Moreover, the consideration of the extra bubble dispersion due to the subgrid scale velocity  $u^{SGS}$  given by eq. (12) has no strong influence and is not able to correct the high bubble mean diameter in the wall region which, of course, has the effect of producing a non-realistic mean bubble velocity peak close to the wall, as pointed out in Laín and Sommerfeld (2004).

Figure 8 shows the liquid fluctuating kinetic energy (top) and the gas fluctuating vertical velocity (bottom). In the scheme followed in this work, the liquid velocity fluctuations are calculated during the simulation as:

$$\overline{u_i u_i} = \frac{n - n_0}{n - n_0} \overline{u_i u_i} + \frac{1}{n - n_0} (u_i^n - \overline{u_i^n})^2 \quad (15)$$

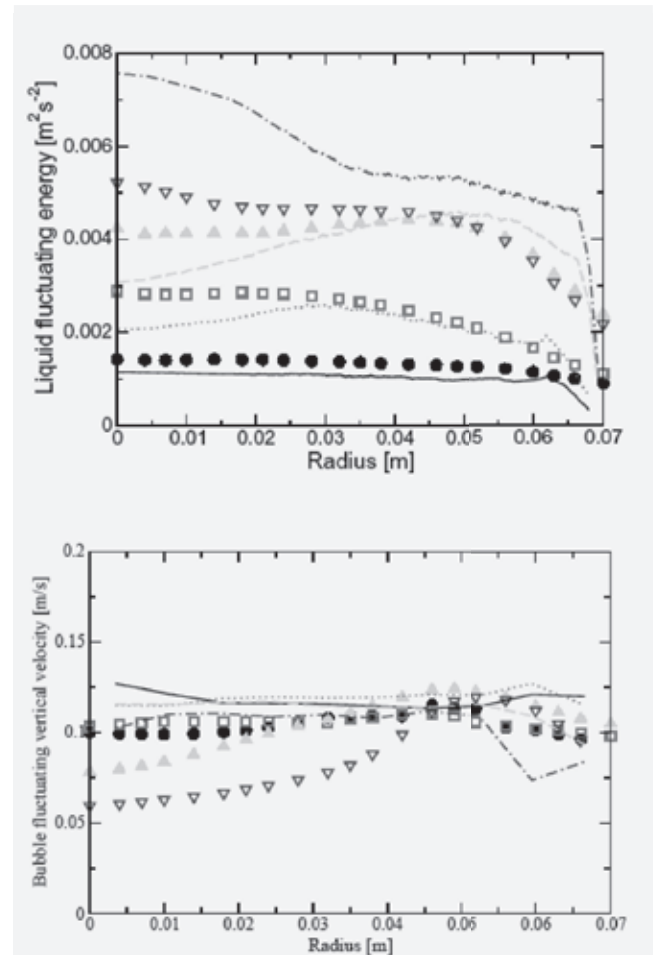


**Figure 8.** Fluctuating kinetic energy of the liquid (top) and vertical fluctuating bubble velocities (bottom) in four cross-sections of the bubble column  $z = 33, 110, 308, 495$  mm.

Considering the upper plot of that figure, it can be seen as the simulated mean liquid fluctuating kinetic energy,  $k = 0.5\overline{u_i u_i}$ , captures fairly well the tendency of the experimental PIV measurements, although there are some discrepancies for the lower cross-sections. However, the calculated values agree reasonably well with the experiments at the highest sections at  $z = 308, 495$  mm. and also in the vicinity of the wall region for the other sections. This behaviour substantially improves the results presented in Laín and Sommerfeld (2004) regarding this variable. Also, the bubble vertical fluctuating velocity compares reasonably well with the experimental data, especially in the upper sections, showing a flat profile without any peak near the wall.

Finally, Figure 9 presents the quantitative comparison between the LES simulations performed for both, fluid and rigid bubbles, the experimental data and the  $k-\varepsilon$  two-dimensional simulations reported in Laín *et al.* (2001) at section  $z = 495$  mm. above the aerator. The upper part of Figure 9 shows that the mean vertical liquid velocities (in black, left vertical axis) provided by the 3D LES calculations are in good agreement with both,

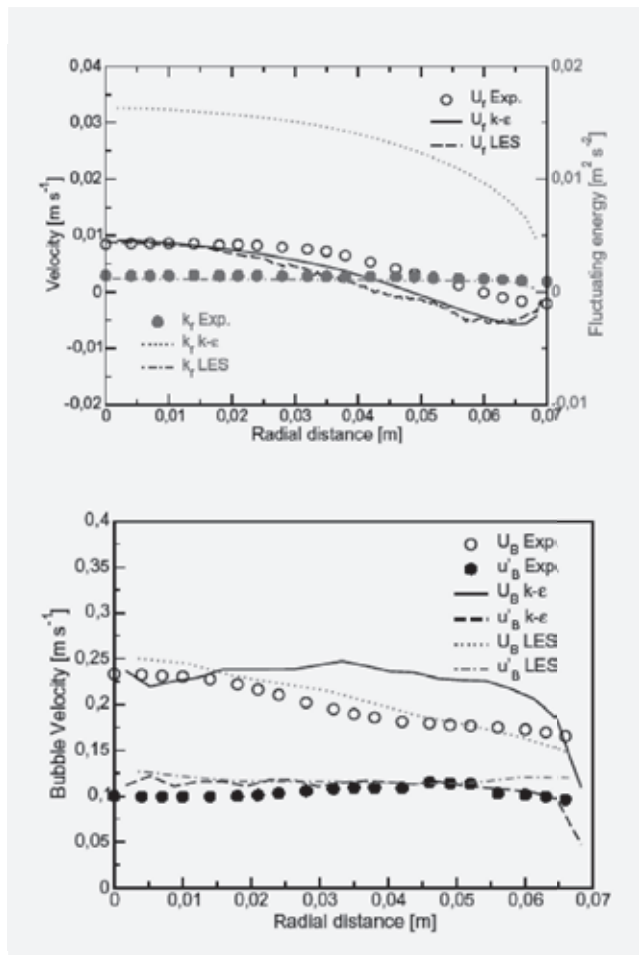


**Figure 9.** Comparison of results for the  $k-\varepsilon$  model and LES against experimental data at section  $z = 495$  mm above the aerator. Fluid variables (top) and Hubble velocities (bottom).

experimental data and results of the  $k-\varepsilon$  turbulence model. Also, the fluctuating kinetic energy of the liquid is shown in the same plot (in red, right vertical axis). Here, it is observed that the LES simulations provide a very good estimation of that variable, improving drastically the result of the 2D simulations performed with the  $k-\varepsilon$  model.

On the other hand, the bubble vertical mean velocity and its fluctuating component are quite similar to the values provided by the  $k-\varepsilon$  model and the experiments, although LES gives a better prediction of the mean velocity. As previously mentioned, this behaviour is due to the nearly even spreading of bubbles across the column, as previously commented.


## Conclusions

In this work results on the simulation of the three-dimensional transient flow developing in a cylindrical laboratory bubble column have been presented. The calculation scheme is based on the combination of Large Eddy Simulation for the liquid phase and a Lagrangian approach for the dispersed gas phase. Previous conclusions available in the literature have been taken into account. Interestingly, the consideration of a simple model to account for the so-called bubble induced turbulence, linked to the subgrid liquid fluctuating velocity, did not modify significantly the performance of the simulation, confirming that this effect does not influence bubble dispersion in this kind of flow configuration.

As in previous works, a strong dependency of the bubble dispersion in the column on the value of transverse lift force coefficient,  $C_{TL}$  has been found. It is concluded that the combination of the transverse lift, which depends on the bubble-liquid relative velocity, and the drag law is the main mechanism responsible for the spreading of the bubbles across the column cross-section.

As a result, the three-dimensional LES simulation reproduces fairly well the dynamic structure of the liquid flow pattern and the long term steady state recirculating flow configuration providing also reasonably good quantitative comparison with the experiments, especially at cross-sections well above the aerator. The obtained results considerably improve those obtained in a previous work (Lain and Sommerfeld, 2004).

## Acknowledgement

This research project is being funded by the Universidad Autonoma de Occidente (Colombia) under reference number 03-PIM-9. This financial support is gratefully acknowledged. 

**Bibliographic**

- Bourloutski, E., Sommerfeld, M. Parameter studies on the three-dimensional calculation of bubble columns. Joint US ASME/European Fluids Engineering Summer Conference, Montreal, Paper No. FEDSM 2002-31218 (2002).
- Bröder, D., Sommerfeld, M. An advanced LIF-PLV system for analysing the hydrodynamics in a laboratory bubble column at higher void fraction. *Experiments in Fluids* 33, 826-837 (2002).
- Crowe, C.T., Sharma, M.P., Stock, D.E. The Particle-Source-in-Cell (PSI-Cell) method for gas-droplet flows. *J. Fluids Eng.* 99, 325-332 (1977).
- Decker, S. Zur Berechnung von gerührten Suspensionen mit dem Euler-Lagrange Verfahren (in German). Ph.D. Thesis, University Martin-Luther Halle-Wittenberg, Germany (2005).
- Deen, N.G., Solberg, T., Hjertager, B.H. Large eddy simulation of the gas-liquid flow in a square cross-sectioned bubble column. *Chem. Eng. Sci.* 56, 6341-6349 (2001).
- Gouesbet, G., Berlemont, A. Eulerian and Lagrangian approaches for predicting the behaviour of discrete particles in turbulent flows. *Prog. Energy Combust. Sci.* 25, 133-159 (1999).
- Jakobsen, H.A., Sannaes, B.H., Grevskott, S., Svendsen, H.F. Modeling of vertical bubbledriven flows. *Industrial and Eng. Chemistry Res.* 36, 4052-4074 (1997).
- Laín, S., Bröder, D., Sommerfeld, M. Numerical simulations of the hydrodynamics in a bubble column: Quantitative Comparisons with experiments. Proc. of the 4th Int. Conf. on Multiphase Flow, May 27 - June 1 2001, New Orleans, USA (2001).
- Laín, S., G'oz, M.F. Numerical instabilities in bubble tracking in two-phase flow simulations. *Int. J. Bifurcation and Chaos* 11, 1169-1181 (2001).
- Laín, S., Bröder, D., Sommerfeld, M., G'oz, M.F. Modelling hydrodynamics and turbulence in a bubble column using the Euler-Lagrange procedure. *Int. J. Multiphase Flow* 28, 1381- 1407 (2002).
- Lain, S., Sommerfeld, M. LES of gas-liquid flow in a cylindrical laboratory bubble column. Proc. 5th Int. Conf. on Multiphase Flow, ICMF 2004, paper No. 337. Yokohama, Japan, May 30 - June 4 (2004).
- Laín, S. Modelado y simulación de flujos inducidos por burbujas. Ed. Universidad Autónoma de Occidente, ISBN 978-958-8122-51-9 (2007).
- Lilly, D.K. The representation of small scale turbulence in numerical simulation experiments. Proc. IBM Scientific Computing Symp. on Environmental Sciences, 320 No. 1951, 195-210 (1967).
- Legendre, D., Magnaudet, J. A note on the lift force on a spherical bubble or drop in a low Reynolds number shear flow. *Phys. Fluids*, 9, 3572-3574 (1997).
- Milelli, M., Smith, B.L., Lakehal, D. Some new approaches to bubble plume modeling using CFD. Proc. Int. Mechanical Eng. Congress and Exposition, New York (USA), November 2001.
- Sanyal, J., Vásquez, S., Roy, S., Dudukovic, M.P. Numerical simulations of gas-liquid dynamics in cylindrical bubble column reactors. *Chem. Eng. Sci.* 54, 5071-5083 (1999).
- Smagorinsky, J. General circulation experiments with the primitive equations. *Monthly Weather Review* 91, 99-165 (1963).
- Tomiya, A. Struggle with computational bubble dynamics. Proc. of the 3th Int. Conf. on Multiphase Flow, June 8-12 1998, Lyon, France (1998).
- Tran, M.L. Modélisation instationnaire de la distribution spatiale des phases dans les écoulements diphasiques en régimes à bulles (in French). Ph.D. Thesis, University Claude Bernard, Lyon (1997).
- V. den Hengel, E.I.V., Darmana, D., Deen, N.G., Kuipers, J.A.M. Large Eddy Simulation of a Bubble Column Reactor using the Euler-Lagrange Approach, Computational Fluid Dynamics in Chemical Reaction Engineering III, May 25-30, 2003, Davos, Switzerland (2003).